Heliyon 8 (2022) e12243

Contents lists available at ScienceDirect

Heliyon

journal homepage: www.cell.com/heliyon

Research article

Biosynthesis of zinc oxide and silver/zinc oxide nanoparticles from *Urginea epigea* for antibacterial and antioxidant applications

Martha Cebile Jobe [a], Doctor M.N. Mthiyane [a,b], Mulunda Mwanza [b,c], Damian C. Onwudiwe [d,e,*]

[a] *Department of Animal Science, School of Agricultural Sciences, Faculty of Natural and Agricultural Sciences, North-West University (Mahikeng Campus), Private Bag X2046, Mmabatho, South Africa*
[b] *Food Security and Safety Focus Area, North-West University (Mahikeng Campus), Mmabatho 2735, South Africa*
[c] *Department of Animal Health, School of Agricultural Sciences, North-West University (Mahikeng Campus), Private Bag X2046, Mmabatho, South Africa*
[d] *Material Science Innovation and Modelling (MaSIM) Research Focus Area, North-West University (Mahikeng Campus), Private Bag X2046, Mmabatho, South Africa*
[e] *Department of Chemistry, School of Physical and Chemical Sciences, Faculty of Natural and Agricultural Sciences, North-West University (Mahikeng Campus), Private Bag X2046, Mmabatho, South Africa*

ARTICLE INFO

Keywords:
Agricultural nanotechnology
Physicochemical properties
Zinc oxide
Silver/zinc oxide
Urginea epigea
Biological activity

ABSTRACT

Zinc oxide (ZnO) and silver-zinc oxide (Ag/ZnO) nanocomposite were synthesized by a green method using $Zn(CH_3COO)_2$ and $AgNO_3$ as precursors for zinc and silver respectively; and *Urginea epigea* bulb extract as a reducing/capping agent. The nanomaterials were characterized by X-ray diffraction (XRD) analysis, Fourier transform infrared spectrophotometer (FTIR), ultraviolet-visible spectrophotometer, scanning, and transmission electron microscopy (SEM and TEM). Their elemental composition was studied using EDX analysis, while elementary mapping was used to show the distribution of the constituent elements. The powder X-ray diffraction confirmed hexagonal phase ZnO, while the Ag/ZnO nanocomposites identified additional planes due to cubic phase Ag nanoparticles. The absorption spectrum of the nanocomposite indicated a red shifting of the absorption band of the metallic ZnO and a surface plasmon resonance (SPR) band's appearance in the visible region due to the metallic Ag nanoparticles. The analysis from the TEM image showed the particles were of spherical morphology with a mean size of 35 nm (ZnO) and 33.50 nm (Ag/ZnO). The biological activity of the nanoparticles was studied for their antibacterial and antioxidant capacity so as to assess their ability to hinder bacterial growth and capture radical species respectively. The results demonstrated that the modification of ZnO with silver nanoparticles enhanced the antibacterial potency but reduced the antioxidant activity. This biogenic method offers a facile approach to nanoparticles for biological purposes, and the strategy may be extended to other metal oxide and their composites with metallic silver nanoparticles as a more effective approach compared to the physical and chemical routes.

1. Introduction

Among the metallic and metal oxide nanomaterials, silver (Ag) and zinc oxide (ZnO) nanoparticles (NPs) are widely used. They have found wide applications in various fields including medicine, renewable energy, cosmetics, textile manufacturing, environmental remediation, electronics, surface disinfection, agriculture, and others. With their large binding energy, high piezoelectric properties, biocompatibility, and non-toxicity, ZnO-NPs have become the subject of intense research due to their increased industrial potential (Jain et al., 2020). Also, Ag-NPs are one of the inorganic nanomaterials of great popularity due to their excellent antimicrobial activity (Senthilraja et al., 2018; Das et al., 2016; Tao et al., 2019). Together with Ag-NPs, ZnO-NPs have proved to be of formidable utility as antimicrobial substances against resistant microbial strains even at very low concentrations (Kim et al., 2007; Sondi and Salopek-Sondi, 2004) due to their intracellular destruction of many biological pathways in microbial cells (Liu et al., 2018; Huh and Kwon, 2011), leading to induction of long-lasting cell growth inhibition within a very short contact time (Gunalan et al., 2012; Feris et al., 2010).

The antimicrobial activity of Ag-NPs is a function of particle size, with higher antimicrobial efficiency as the size decreases (Morones et al., 2005; Samberg et al., 2011). However, the problem of NPs aggregation ensues as Ag-NPs size decreases, leading to the decreased antibacterial activity of the NPs. Consequently, this has led to the recent hybridization innovation of

* Corresponding author.
E-mail address: damian.onwudiwe@nwu.ac.za (D.C. Onwudiwe).

https://doi.org/10.1016/j.heliyon.2022.e12243
Received 24 May 2022; Received in revised form 28 August 2022; Accepted 1 December 2022

incorporating Ag-NPs into various other nanomaterials including ZnO to prevent aggregation as well as cytotoxicity of the former (Agnihotri et al., 2015; Ocsoy et al., 2013). In addition, Ag/ZnO hybrid NPs have been shown to have further enhanced antimicrobial activity compared to the individual capabilities of their components (Gupta et al., 2017). The enhanced properties of Ag/ZnO-NPs derive from the synergy between the two NPs (Youssef et al., 2017), which augments oxidative stress induction and hence improves the antimicrobial activity of the nanocomposite (Liu et al., 2020; Lu et al., 2017; Rajaboopathi and Thambidurai, 2019).

Recently, ZnO-NPs have found animal feed safety and animal health applications emanating from their newfound utility in binding mycotoxins. In this regard, Saramas and Ekgasit demonstrated the ability of high surface-area-activated carbon with ZnO-NPs to bind the mycotoxins aflatoxin B1 (AFB1), zearalenone, and fumonisin B1, and that this nano product could be used as an animal feed additive (Saramas and Ekgasit, 2021). However, this composite of carbon with ZnO-NPs was synthesized using a non-green approach involving potentially toxic chemicals and therefore may not be biologically friendly.

In farm animals, particularly pigs and chickens, mycotoxins induce acute to chronic effects including carcinogenicity, mutagenicity, teratogenicity, immunosuppression, and endocrine disruption (Milićević et al., 2010; Haque et al., 2020) with the predisposition of animals to secondary bacterial infections (Pierron et al., 2016). Their toxicity is mediated through induction of oxidative stress and compromising of the animal's antioxidant defence mechanisms (Mavrommatis et al., 2021) as is the case with bacterial infections (Lauridsen, 2019). Unfortunately, there is currently no remedy for mycotoxin infections in farm animals and human beings. Instead, mycotoxin binders have been incorporated into animal diets as a strategy to bind mycotoxins to render them unavailable for interaction with the animal's digestive and cellular systems. However, these substances have lately been shown to also sequester and thus decrease the bioavailability of dietary nutrients including proteins, amino acids, vitamins (Kihal et al., 2021; Barrientos-Velázquez et al., 2016) and also in-feed antibiotics (Goossens et al., 2012). Since the mechanism of action of mycotoxins generally involves induction of cellular or tissue oxidative stress, there is, therefore, an urgent need for an alternative antioxidant-bolstering strategy to attenuate their toxicity in farm animals.

One possible mycotoxin ameliorative strategy involves the administration of plant-derived bioactive compounds (phytochemicals) that have the capacity to increase the gene expression and specific activity of enzymes. They can defend cells and tissues against oxidative stress as well as be involved in the biotransformation of mycotoxins and their epoxides. Such enzymes include glutathione S-transferase (GST) (Hayes et al., 1991a, 1991b; Guengerich et al., 1998) and heme oxygenase (Milbury et al., 2007). In this regard, studies have shown that pre-treatment with plant-derived GST isoform inducers protects against DNA damage and carcinogenesis induced by aflatoxin B1 (AFB1), one of the mycotoxins (Buetler et al., 1995; Manson et al., 1997). Also, other researchers have shown that *in vivo* administration of phytochemicals upregulates gene expression and the activity of heme oxygenase (Milbury et al., 2007) and ameliorates AFB1-induced effects via up-regulation of antioxidant enzyme gene expressions, and increase the availability of reduced glutathione (GSH) (El-Bahr, 2015; Limaye et al., 2018; Lee et al., 2019) the major antioxidant in all living cells.

It is against this background that phytochemicals of plants such as *U. epigea* are being investigated for their ability to bolster antioxidant mechanisms in animals and poultry subjected to mycotoxin toxicity. An indigenous bulbous plant inhabiting semi-arid and rocky grasslands of many Southern African countries of the eastern seaboard, and commonly used by Zulu, Swati, and Xhosa traditional healers as an oral tonic for soothing body pains, healing bone fractures, and as an aphrodisiac. The plant is reported to possess cardiotonic activity and its bulb sap usually induces skin irritation upon handling. This is due to the presence mainly of bufadienolides (Koorbanally et al., 2004; Lukhoba et al., 2006). Bufadienolides are a group of 24-carbon cholesterol-related polyhydroxy steroids and their glycosides; they are characterized by a six-membered doubly unsaturated lactone ring as well as a 2-pyrone group at the C-17 position of the perhydro phenanthrene nucleus (De Sousa et al., 2017; Kolodziejczyk-Czepas and Stochmal, 2017). They have blood pressure stimulating, anti-angiogenic, anti-viral, immunomodulatory, anti-inflammatory, and antibacterial activities (Gao et al., 2011; Kamboj et al., 2013; Xiao et al., 2011; Wu and Lu, 2022).

Nonetheless, phytochemicals are chemically unstable and easily degradable upon exposure to conditions like temperature, oxygen, pH, and light before being absorbed (Assadpour and Mahdi Jafari, 2019). Therefore, it is necessary to protect these bioactive compounds to ensure their controlled release at the target site. Encapsulation of phytochemicals into NPs through biogenic NP synthesis is one of the most effective techniques for entrapping, protecting, and delivering bioactive materials into biological systems (Dima et al., 2020; Koshani and Jafari, 2019; Rezaei et al., 2019). They can induce skin irritation upon handling (Koorbanally et al., 2004), are hydrophobic, and possess weak antioxidant potential (Kolodziejczyk-Czepas and Stochmal, 2017). These properties might limit their direct addition into animal feed formulations. Bufadienolides are ideal phytochemical candidates for nanoencapsulation. However, no studies have previously investigated nanoencapsulation through phytogenic synthesis of ZnO and Ag/ZnO NPs mediated by *U. epigea* phytochemicals. Also, no studies have reported the antioxidant and antibacterial applications of these NPs. The objective of this study therefore was to study the biosynthesis, physico-chemical characteristics, as well as antibacterial and antioxidant activities of *U. epigea* bulb extract-mediated ZnO and Ag/ZnO NPs. Furthermore, the pristine ZnO and the composite with Ag were also prepared using the conventional method, without the green plants, and a comparison of their optical, structural, as well as morphological properties were made.

2. Materials and methods

2.1. Materials

Urginea epigea bulbs were collected at Ermelo, Mpumalanga province, South Africa at a latitude of -26° 31′59.99″ S and longitude of 29° 58′59.99″ E. Zinc acetate dihydrate ($Zn(CH_3COO)_2 \bullet 2H_2O$) and silver nitrate ($AgNO_3$) were procured from Merck. Sodium hydroxide (NaOH), ethanol, 3-(4, 5- dimethylthiazol-2-yl)-2, 5-diphenyltetrazolium bromide (MTT), dimethyl sulfoxide, and Ascorbic acid were obtained from Merck. All chemicals were used as received.

2.2. Instrumentation

The XRD samples were recorded using the Bruker D8 Advance, which was equipped with a counter that uses CuKα radiation (k = 1.5405, nickel filter) and operated at 40 kV and 40 mA. The FTIR spectrum of the *U. epigea* bulb was acquired on a Cary 670 FTIR spectrometer. The absorbance properties of synthesized *U. epigea* ZnO and Ag/ZnO nanoparticles were measured on a Cary 30 UV–vis spectrometer from Agilent technologies. A TECNAI G2 transmission electron microscope (TEM) was used to study the morphology of the nanoparticles at an accelerating voltage of 200kV. Image J software was used on the TEM images to determine the average particle size of the nanoparticles.

2.3. Extraction of the phytocomponents from the U. epigea bulb

The collected bulb was rinsed under a running tap, afterwards by distilled water to remove dust and unwanted specks of dirt. These bulbs were chopped, air-dried under shade to prevent the volatile organic component from escaping, and grounded to powder. The biomolecules were extracted from the plant by adding 5 g of bulb powder into 100 mL of distilled water and heated at 80 °C for 4 h, while continuously stirring with a magnetic stirrer. The mixture was cooled to room temp., filtered, and the obtained filtrate was stored at 4 °C for further use.

2.4. Synthesis of zinc oxide nanoparticles

0.05 M of $Zn(CH_3COO)_2$ was utilized for the preparation of ZnO-NPs following an already described procedure (Thema et al., 2015). About 20

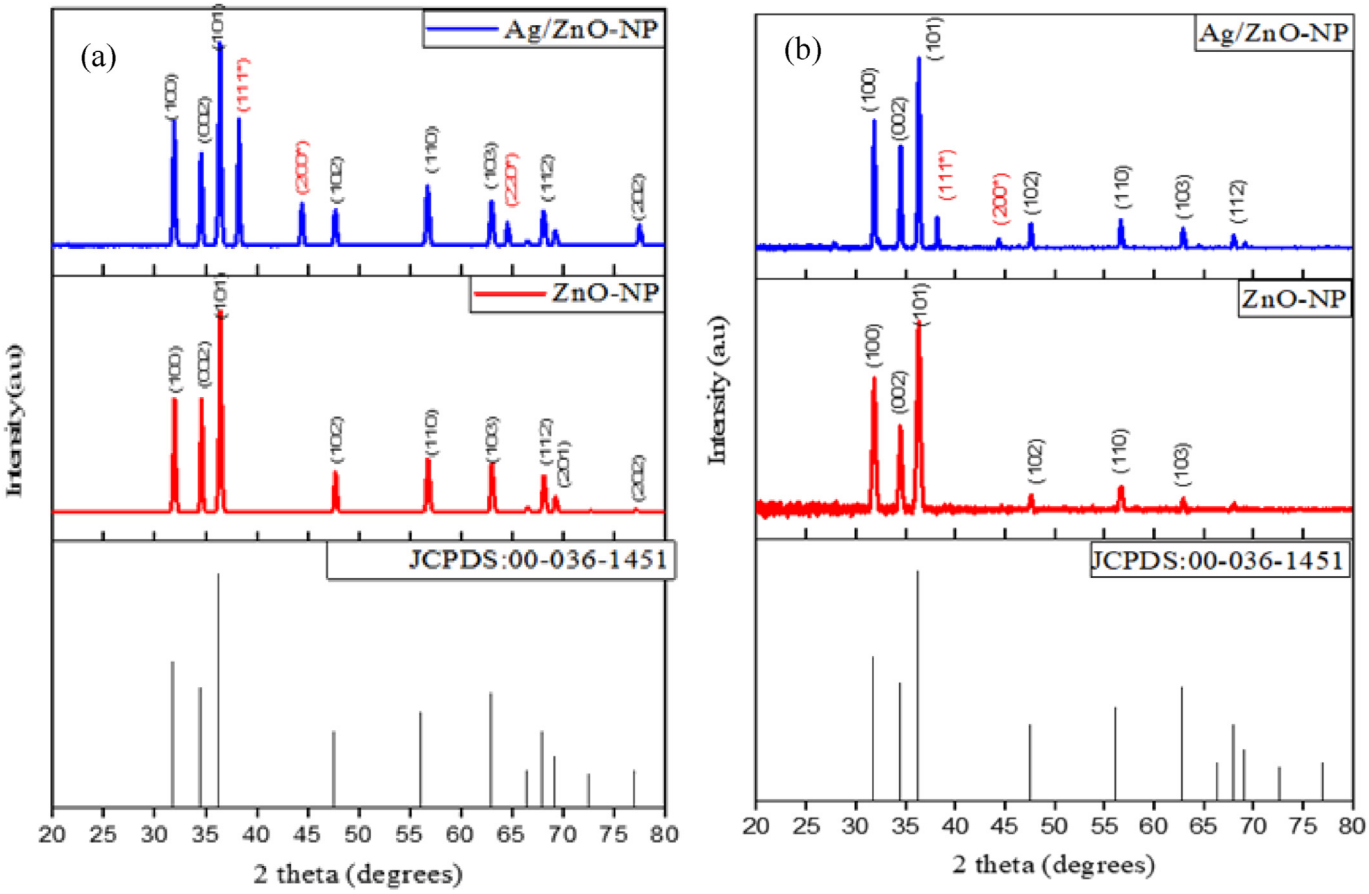

Figure 1. XRD patterns of ZnO and Ag/ZnO-NPs synthesized using (a) conventional (b) green method.

mL of the aqueous extract of *U. epigea* was mixed with 0.05 M of Zn $(CH_3COO)_2$ solution and the pH was adjusted to 8 by adding a solution of 2.0 M sodium hydroxide in dropwise, followed by vigorous stirring at 85 °C for 2 h. The colour change from brown to creamy white after 40 min signalled the formation of the nanoparticles, and therefore the reaction was terminated. The solution was then cooled and centrifuged for 30 min at 4300 rpm to separate the precipitate. The collected precipitate was rinsed three times with distilled water and ethanol, then dried overnight at room temperature before being calcined at 400 °C for 3 h to afford the nanoparticles.

2.5. Synthesis of Ag/ZnO nanocomposite

For the Ag/ZnO-NPs, 0.05 M Zn $(CH_3COO)_2$ was mixed with 0.2% Ag/NO_3 and stirred steadily on a magnetic stirrer. Thereafter, a solution of NaOH was added in dropwise to adjust the pH to 8. The solution was heated at 85 °C for 15 min, then about 20 mL of plant extract was added and the reaction was left for 90 min. The mixture was allowed to cool to room temp. and the composite was recovered by centrifuging for 30 min at 43000 rpm. Afterwards, the product was rinsed three times with distilled water and ethanol, dried at 50 °C for 3 h, and was calcined at 450 °C for 2 h. The nanoparticles were then stirred overnight in a solution of the plant extract to allow the interaction of the nanoparticles with the plant's biomolecules. The product was then filtered, dried in the air, and transferred into a sealed container for characterization.

2.6. Antibacterial testing of ZnO nanoparticles and Ag/ZnO nanocomposite

The bacterial strains used were Gram-positive (*Klebsiella oxytoca, Staphylococcus aureus*, and *Bacillus cereus*) and Gram-negative (*Escherichia coli*). The antibacterial screening was carried out using the agar disk diffusion method. Muller–Hinton agar was used to prepare the Petri plates. The test cultures at a concentration of 106 CFU/mL were streaked onto condensed agar in Petri dishes by the aid of a sterilized cotton swab and allowed to dry for 15 min. For the nanoparticles that were evaluated, 100% dimethyl sulfoxide was employed as a diluent. ZnO and Ag/ZnO concentrations of 5, 7.5, and 10 μg/mL were soaked in a 6.0 mm diameter blank paper disks. After incubation at 37 °C for 30 min, each plate was stained purple with 1.25 mg/mL 3-(4, 5- dimethylthiazol-2-yl)-2, 5-diphenyltetrazolium bromide MTT (Merck). For the bacteria, the plates were allowed to incubate for 24 h at 37 °C, and control studies were conducted under comparable conditions using commercially available antibacterial drugs as positive control drugs and 100 % DMSO as a negative control. The diameters of inhibitory zones were measured to determine the microorganism species sensitivities to the samples. The experiment was done twice, and the inhibition zones were measured in mm.

2.7. Antioxidant activity of ZnO nanoparticles and Ag/ZnO nanocomposite

The antioxidant potency of the ZnO and Ag/ZnO was determined using the DPPH technique. Briefly, 1 mL of 100 M DPPH was prepared in methanol and mixed with 1 mL of ZnO and Ag/ZnO-NPs solution (concentrations of 20, 40, 60, 80, and 100 μg/mL) before being dispersed in methanol. Ascorbic acid was used as a standard with the same concentrations as ZnO and Ag/ZnO-NPs. Both the control and sample absorbances were read at 520 nm, and the experiment was repeated three times. DPPH scavenging activity was determined using the formula shown in Eq. (1):

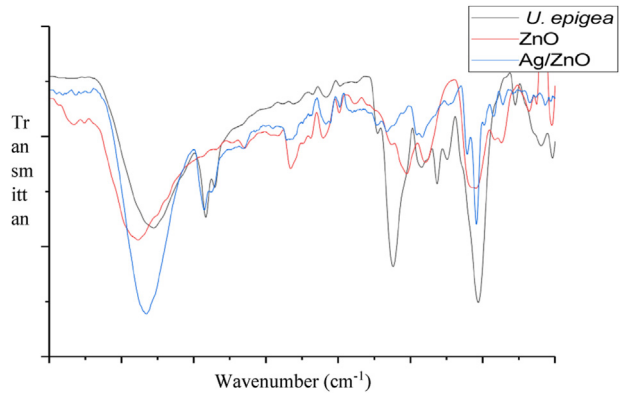

Figure 2. FTIR of *U. epigea* bulb, ZnO, and Ag/ZnO nanoparticles.

$$\text{Scavenging activity\%} = \frac{\text{Absorbance control} - \text{Absorbance sample}}{\text{Absorbance control}} \times 100 \quad (1)$$

3. Results and discussion

3.1. XRD patterns of ZnO nanoparticles and Ag/ZnO nanocomposite

The purity and crystallinity of the ZnO and Ag/ZnO were studied using XRD analysis and are shown in Figure 1. The peaks which appeared at 31.67°, 34.46°, 36.32°, 47.50°, 56.66°, 62.93°, and 67.85° for ZnO nanoparticles in Figure 1 corresponded to (100), (002), (101), (102), (110), (103), and (110) crystallographic planes respectively of hexagonal phase ZnO (JCPDS No: 00-036-1451). The diffraction pattern of the ZnO NPs from the two routes: conventional (Figure 1a) and green (Figure 1b) showed a difference in the peak intensity, specifically in the (0 0 2) plane, which might indicate a difference in the growth direction of the nanoparticles. The introduction of Ag to ZnO to form a composite showed additional diffraction peaks to the ZnO patterns at 31.7°, 34.8°, 36,1°, 38.5°, 38.0°, 44.2°, 47.5°, 56.9°, 62.7°, and 67.9° attributed to the crystallographic phase of cubic planes of Ag. Characteristic peaks of the Ag appeared at 2θ = 38.0°, 44.2°, and 64° which confirmed that silver was present in the Ag/ZnO composite. The intense diffraction peaks affirm the significant increase in crystallinity of the ZnO in the Ag/ZnO composite compared to ZnO alone, and this could be ascribed to the higher temperature of calcination in the latter. Debye Scherer's Eq. (2) was used to estimate the average crystallite size of the nanoparticles.

$$D = k\lambda/\beta \cos\theta \quad (2)$$

where D is the crystallite size, β is the FWHM, depicting the Full width at half maximum measured in radians, K is a constant (0.90), which is known as the Scherrer shape factor, λ represents the X-ray wavelength (1.5406Å), and θ is the Bragg diffraction angle, which is given in degrees. The estimated particle sizes of the conventional ZnO and Ag/ZnO (30.8 and 30.4 nm) were higher than biosynthesised ZnO and Ag/ZnO (25.09 and 25.16 nm) NPs respectively.

3.2. Infrared spectral studies of U. epigea bulb and the synthesized nanoparticles

FTIR was used to explore the possible functional groups of the biomolecules present in the *U. epigea* bulb. In the FTIR spectrum presented in Figure 2, the major absorption bands appeared at 3294, 2919, 1612, 1317, and 1035cm^{-1}. The observed broad peak at 3294 cm^{-1} could be

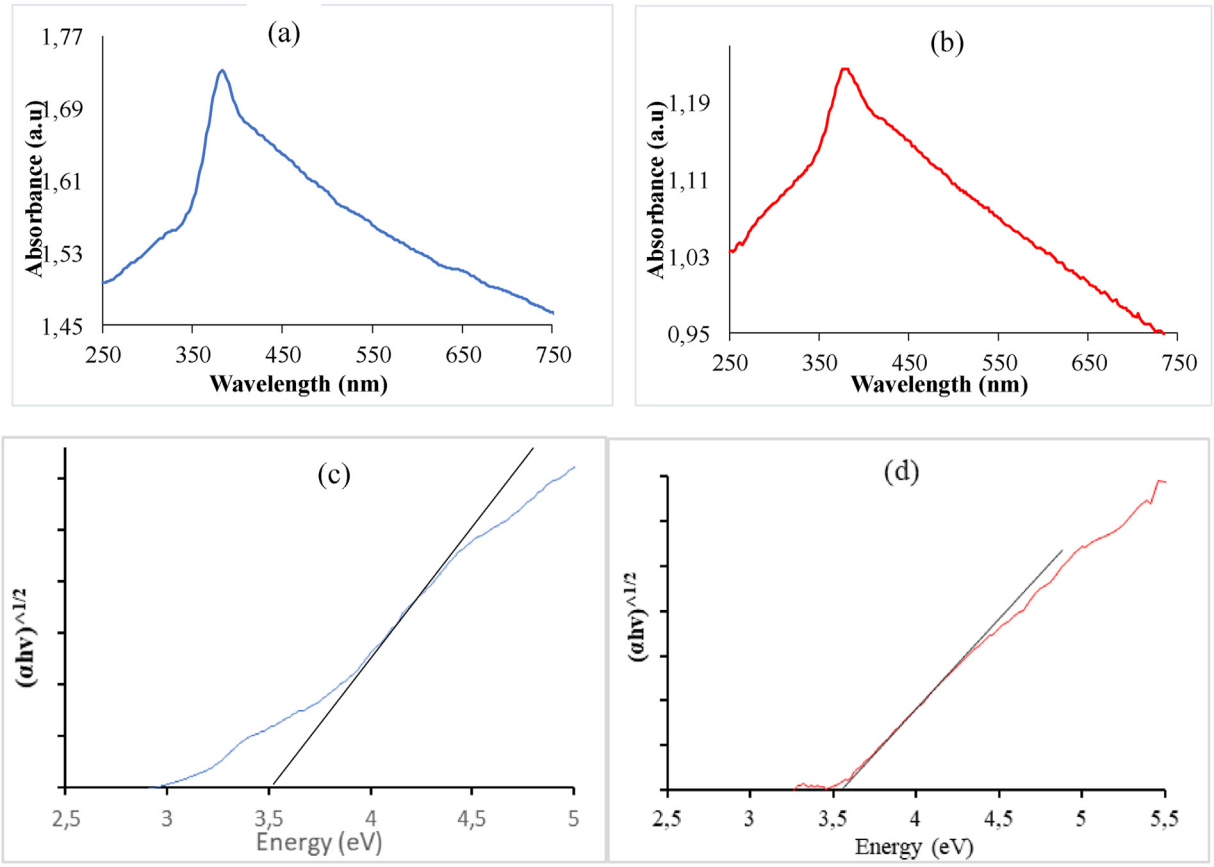

Figure 3. UV-vis spectra of (a) conventional and (b) biosynthesized ZnO; and Tauc plot showing respective bandgap energy of conventional (c) and biosynthesized (d) nanoparticles.

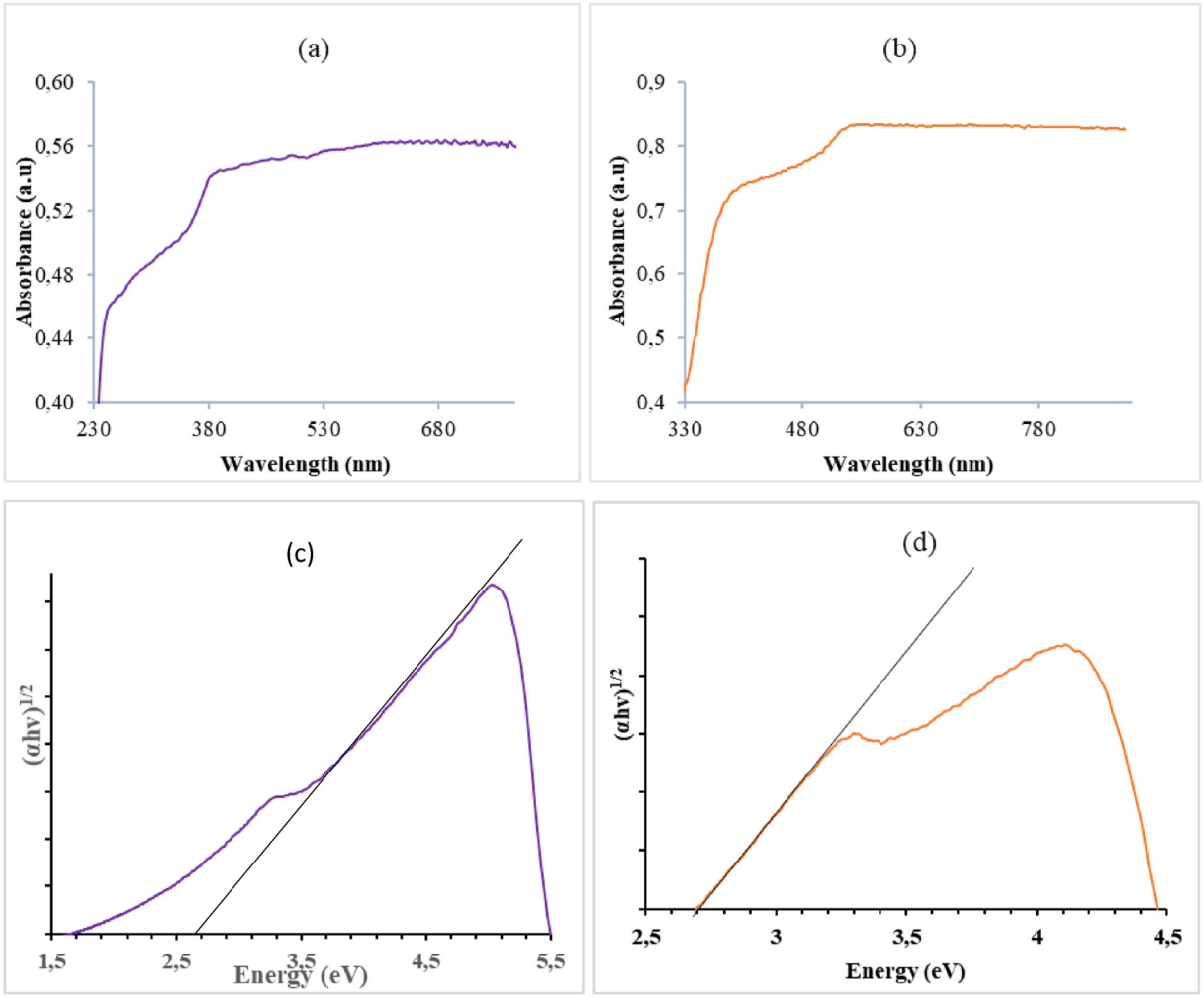

Figure 4. UV-vis spectra of (a) conventional and (b) biosynthesized Ag/ZnO; and Tauc plot showing bandgap energy of conventional (c) and biosynthesized (d) Ag/ZnO nanoparticles.

attributed to the O–H stretching vibration (Ajitha et al., 2015). The two low-intensity peaks at 2919 cm^{-1} and 2879 cm^{-1} were the symmetric and asymmetric C–H of the alkane group (Álvarez-Chimal et al., 2022). The peak at 1612 cm^{-1} is attributed to C=C stretching vibration (Jayachandran et al., 2021), while the C–O- vibrations appeared around 1035 cm^{-1} (Dobrucka and Długaszewska, 2016). These vibrational frequencies suggest the availability of different biologically active phytomolecules on the nanoparticles that are available for adsorption, which can mediate the synthesis of the nanoparticles from their respective metal salts. The spectra of the ZnO and Ag/ZnO NPs show the presence of peaks identified in the spectrum of the plant extract but with a slight shift in the positions of their appearance and this could be a result of the interaction of the functional groups with the nanoparticles.

3.3. UV-visible studies of ZnO nanoparticles and Ag/ZnO nanocomposite

The optical absorption properties of ZnO nanoparticles prepared via conventional and green methods were studied in the range of 200–850 nm at room temp., and the spectra are shown in Figure 3a and b respectively. The maximal absorption peak of the ZnO nanoparticles in the UV–vis spectral range is around 390 nm. These peaks could be attributed to the absorption engendered by electrons transitioning from the lower valence band to the higher conduction band. Furthermore, these sharp peaks are due to the existence of the particles within the nanosized regime. It could also be indicative of a narrow particle size distribution (Zak et al., 2011). The broadening of the peak as they tailed out could imply polydispersity in the solution (Zhang, 2008). These results corroborate previous reports (Jain, 2013; Selvarajan, 2013; Bajpai, 2016). Figure 4 shows the absorption spectrum of the Ag/ZnO sample. A lower intensity in the light absorption capacity could be observed in the UV range of the spectrum, which broadens out into the visible region. A similar observation has been reported in the biogenic synthesis of Ag/ZnO nanoparticles using extracts of *Crataegus monogyna* (Fouladi-Fard et al., 2022). This is owing to the wide bandgap (3.4 eV) of ZnO which upon addition of Ag nanoparticles to form a composite resulted in red-shifting of the absorption band due to surface plasmon resonance (SPR) (K.K. Paul, 2017). It is possible that the light excitation of the composite generated more electron-hole pairs in the region which resulted in the broadening of the peak. The optical band gap energy of the nanoparticles was determined using the following Eq. (3):

$$\alpha h\nu = A(h\nu - Eg)^{n} \quad (3)$$

where α denotes absorption coefficient, h is Plank's constant, and *ν* represents the frequency of the photon. The symbol A is a constant, while Eg represents the optical band gap energy of the nanoparticles, and the value of n is ½, used when the semiconductor has a direct band gap. The peak maxima in the absorbance spectrum is clearly shown to correlate to the real optical band gap of the ZnO-NPs with an energy band gap of 3.5 eV (Figure 3c and d). Figure 4a and b show the absorption spectra of conventional and biosynthesized Ag/ZnO nanoparticles respectively. The

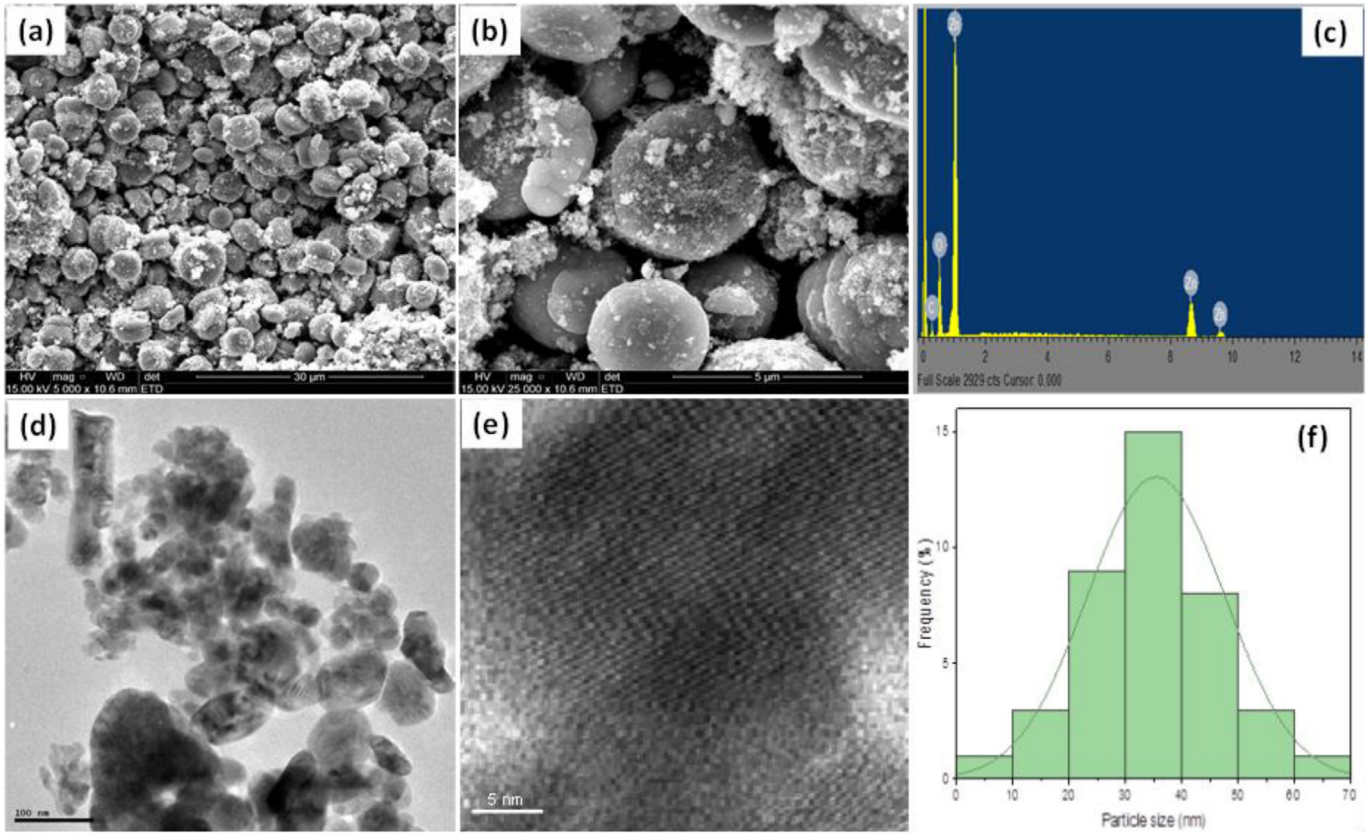

Figure 5. SEM images of the biosynthesized ZnO at (a) low, (b) high magnifications, and (c) EDX spectrum; and the TEM images (d) and its particle size distribution histogram (f).

band gap in ZnO was found to reduce to about 2.6–2.7 eV after the addition of silver (Figure 4c and d respectively). The lowered band gap energy of the composite and widening of absorption range indicate an improvement in the light capturing ability due to the co-addition of Ag and ZnO NPs. It also demonstrates the suitability of the composite for medical applications that require light absorption such as sunscreen protectors and antibacterial ointments.

3.4. Morphological studies of biosynthesized nanoparticles from U. epigea bulb extract

The morphologies of the ZnO-NPs and Ag/ZnO nanocomposites were analysed using SEM and TEM. Figure 5 presents the SEM images of the nanoparticles, where the spherical structures of the ZnO nanoparticles are well distinct at low (Figure 5a) and higher magnifications (Figure 5b). The elemental composition of the samples was studied using EDAX analysis, which confirmed that the pristine ZnO was composed of zinc and oxygen (Figure 5c). Zinc had three strong signals at 1 keV, 8,6 keV, and 9,3 keV, while oxygen signals appeared at 0.6 keV [58]. The internal morphology presented by the TEM micrograph (Figure 5d) corroborated the SEM image, depicting the nanoparticles to be of pseudo-spherical morphology, whose good crystallinity was confirmed by the distinct lattice fringes observable in the HRTEM image of Figure 5e. Particle size distribution histogram (Figure 5f) showed that the average size of the synthesized ZnO NPs were about 33.0 nm.

Figure 6a, b and c are the SEM images of the conventional Ag/ZnO at low and high magnification, as well as the EDX spectrum. The morphology of the Ag/ZnO nanocomposite depicts spherical nanoparticles, and the introduction of the Ag ions did not seem to affect the external morphology of the resulting nanocomposite. The presence of Ag ion within the composite material was confirmed by the EDX spectrum of Figure 6c, which depicts the presence of Ag, Zn and O. The SEM micrographs of the Ag/ZnO using the plant extract (Figure 6d and e) present irregularly distributed short rods with no specific ordering, but with more compactness compared to the unmodified ZnO nanoparticles.

A confirmation of the incorporation of Ag nanoparticles into the modified ZnO is evident in the EDX spectrum of the nanocomposite (Figure 6f). A high-intensity zinc peak at 1 keV (typical peaks at 8,7 keV and 9,5 keV), oxygen (0,5 keV and 2,4 keV), and Ag peak at 3 keV.

The different elemental components of the nanoparticles were evenly and uniformly distributed across the entire nanomaterials as confirmed in Figure 7(a, b, c, d, e, f, g).

TEM analysis of conventional and biosynthesized Ag/ZnO-NPs displayed spherical-shaped images with some degree of agglomeration as presented in Figure 8a and b respectively. The dense parts of the images are possibly due to aggregation and overlapping of smaller particles. There is obvious formation of irregular morphology with different particle sizes, and an average particle size of 27.0 nm for the Ag/ZnO nanoparticles obtained conventionally (Figure 8c). The biosynthesized Ag/ZnO NPs exhibited particles whose size was in the range of 15.0–55.0 nm and an average particle size of 33.50 nm (Figure 8d).

3.5. Antibacterial and antioxidant activity of U. epigea bulb extract mediated ZnO and Ag/ZnO nanoparticles

3.5.1. Antibacterial activity

Generally, ZnO and Ag/ZnO possess some antibacterial properties, which has resulted in their huge application in medicine and other fields (Agarwal et al., 2017). Table 1 depicts the results of the antibacterial activity of both ZnO and Ag/ZnO against selected gram-positive and gram-negative bacterial pathogens. The nanoparticles were observed to be effective against all tested bacterial strains. However, the control drug exhibited higher activity compared to both ZnO and Ag/ZnO NPs. Among

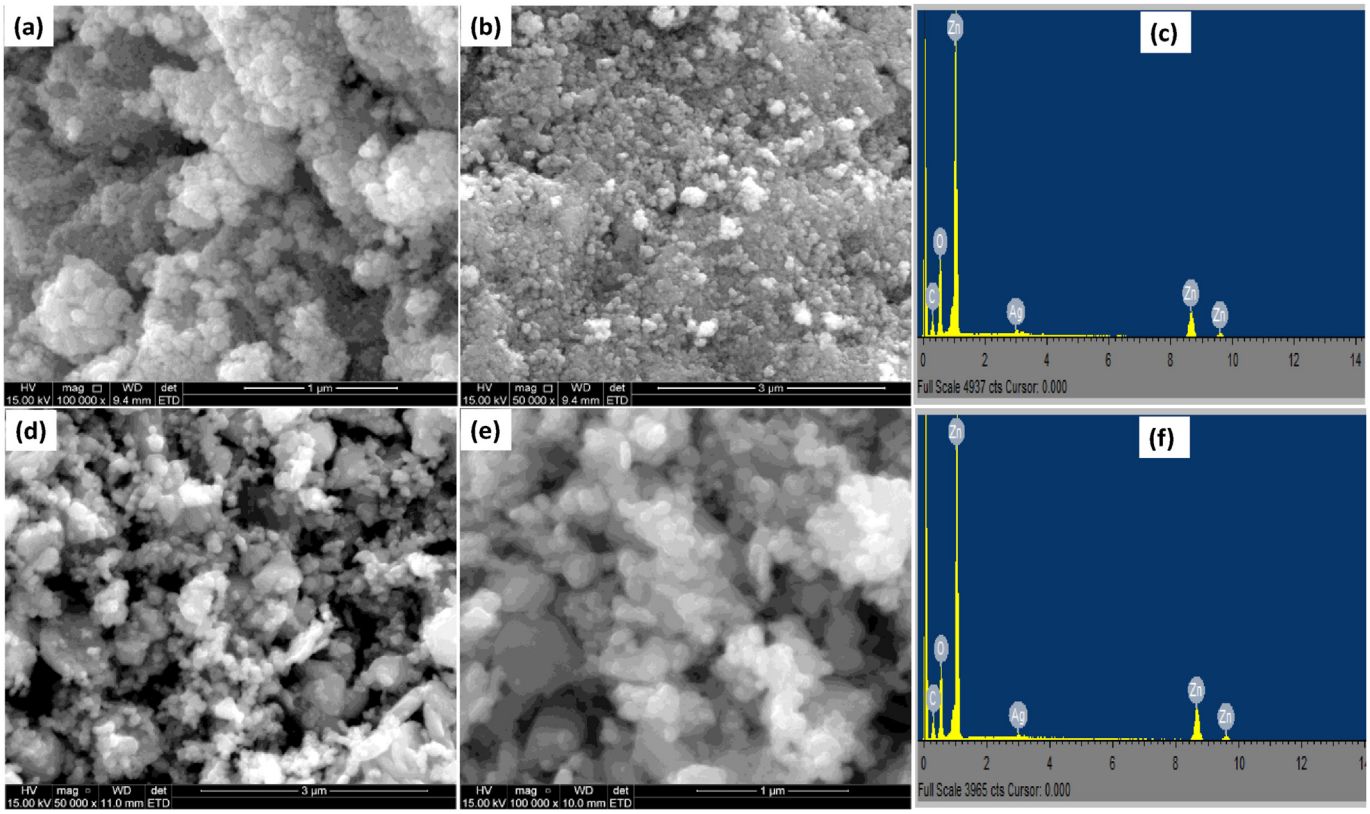

Figure 6. SEM images of the conventional Ag/ZnO at (a) low magnification, (b) high magnification, and (c) EDAX spectrum; and the SEM images of the bio-synthesized Ag/ZnO at (d) low, (e) high magnification, and (f) EDAX spectrum.

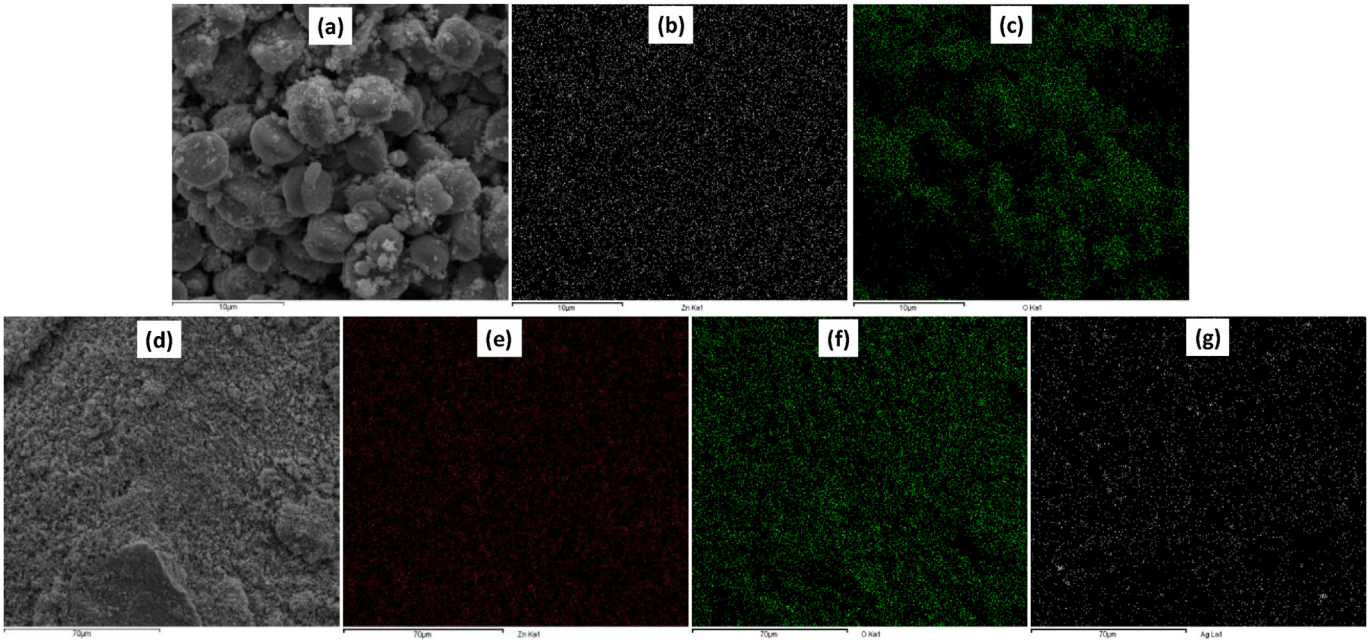

Figure 7. (a) Elemental mapping results of ZnO, (b) Zn, and (c) O elements of ZnO; and the (d) elemental mapping of Ag/ZnO, (e) Zn, (f) O and (g) Ag elements of Ag/ZnO synthesized using extract of *U. epigea* bulb.

the bacterial strains, *E. coli*, and *K. oxytoca* were more susceptible to both test samples than the *S. aureus* and *B. cereus* bacterial strains. Gram + ve bacteria have a rigid cell wall network that makes them resistant to rupture, whereas Gram -ve bacteria have a network of cell membrane that is made up of one molecule thick (Satyavani et al., 2011). Furthermore, the size of nanoparticles has been linked to increased permeability through bacterium cells of *E. coli* (Elemike et al., 2017). However, the Gram + ve bacteria's strengthened cell wall renders it less permeable than the Gram-negative bacteria's cell membrane, as observed with *S. aureus* and *B. cereus*.

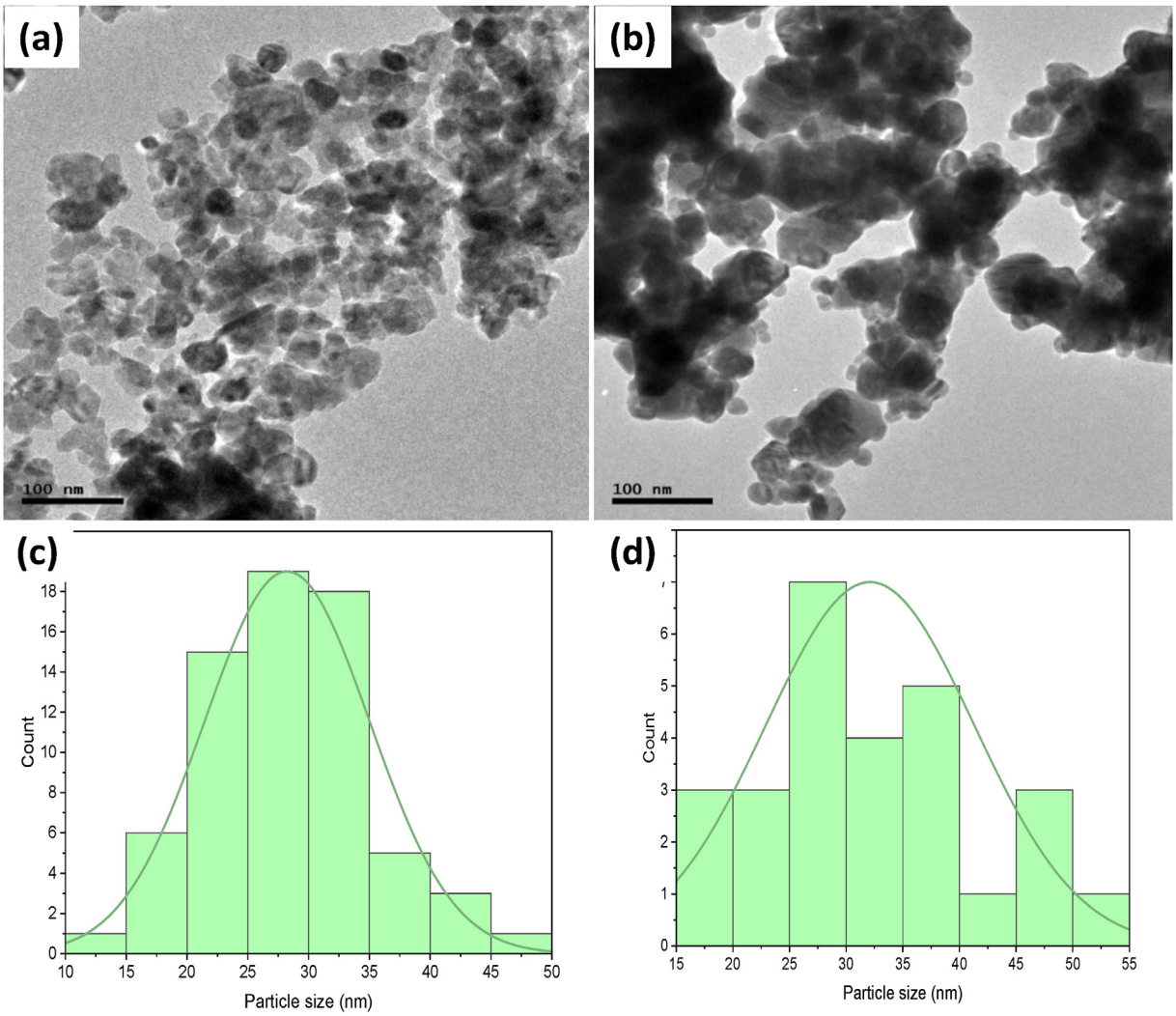

Figure 8. TEM images of Ag/ZnO (a) conventional, (b) biosynthesized 20 mL aqueous extract of *U. epigea* bulb, and their respective particle size distribution histogram (c) and (d).

Table 1. Antibacterial activity of biosynthesised ZnO nanoparticles and Ag/ZnO nanocomposite.

Microorganisms	Inhibition zone (mm) at different a concentration of NPs (μg/mL)							
	ZnO				Ag/ZnO			
	Control	5	7.5	10	Control	5	7.5	10
E. coli	24 ± 0.0	10 ± 0.5	12 ± 0.3	15 ± 0.3	28 ± 1.4	11 ± 0.0	15 ± 1.4	19 ± 0.7
K. oxytoca	20 ± 0.3	9.0	11 ± 0.0	15 ± 0.7	27 ± 0.0	9.0 ± 0.7	1 4 ± 0.3	17 ± 0.7
S. aureus	20 ± 0.7	7.0 ± 0.0	11 ± 0.0	13 ± 0.3	21 ± 0.7	11 ± 0.0	11 ± 0.3	13 ± 0.3
B. cereus	20 ± 0.7	0.0 ± 0.0	9.0 ± 1.4	9.0 ± 0.3	21 ± 0.7	6.0 ± 0.3	9.0 ± 0.7	9.0 ± 0.3

Zone of inhibition mean ± Standard deviation.

Tables 2 and 3 present some selected results of the antibacterial and antioxidant activities of ZnO and Ag/ZnO NPs respectively from different plant extracts reported in the literature. The biosynthesized nanoparticles using different parts of plants display varying degrees of potency against the different pathogenic bacteria including *Escherichia coli*, *Pseudomonas aeruginosa, Streptococcus pneumoniae Bacillus subtilis, Klebsiella pneumonia, Enterococcus faecalis, Staphylococcus aureus, Proteus mirabilis, pyogenes, Proteus mirabilis, Salmonella typhi,* etc (Ramesh, 2015; Happy et al., 2019; Noohpisheh et al., 2020; Taha et al., 2020). They also exhibited moderate to high antioxidant activities. A comparison of these biological activities with results in the current study involving the extract of *Urginea epigea* confirms the high efficacy of green synthesized ZnO and Ag/ZnO NPs against both gram-positive and gram-negative bacteria. The antibacterial property of the ZnO NPs from extract of *Urginea epigea* exhibited a high minimum inhibition concentration against Gram-negative *E. coli* and Gram-poitive *S. aureus* (Bala, 2015). Bhuyan et al. (2015) reported the antibacterial potency of biosynthesized ZnO nanoparticles against *S. aureus*, *S. pyogenes,* and *E. coli* that exhibited a decrease in the growth of bacterial with a concentration 100 μg mL^{-1}.

According to Divya et al. (2013), the mechanism of action for both Ag and ZnO NPs involves the penetration and damage of the bacterial membranes as a result of the production of reactive oxygen species

Table 2. Comparison of the antibacterial and antioxidant activities of ZnO from different plant extracts with other reported studies.

Type of plants extract	Size of nanoparticles	Type of bacteria	Antioxidant assay	Efficiency	References
Ailanthus altissima fruits extract	5.0–18.0 nm	- *Escherichia coli*	-	*E. coli* ++	(Awwad et al., 2020)
		- *Staphylococcus aureus*		*S. aureus* +	
Aloe vera	40.0–180.0 nm	- *Bacillus subtilis*	-	*B. subtilis* ++	(Sharma et al., 2019)
		- *Escherichia coli*		*E. coli*+	
		- *Staphylococcus aureus*		*S. aureus* +	
Aloe vera peel extract	50–220 nm	- *Staphylococcus epidermidis*	-	*E. coli* ++	(Chaudhary et al., 2018)
		- *Klebsiella pneumoniae*		*K. pneumoniae* +	
		- *Escherichia coli*		*S. epidermidis* +	
Aloe socotrina leaf extract	15–50 nm	- *Escherichia coli* (ATCC)	-	*E. coli* ++	(Fahimmunisha et al., 2020)
Azadirachta indica (L.) leaf extract	18.0 nm	- *Staphylococcus aureus*	-	*S. aureus* ++	(Elumalai and Velmurugan, 2015)
		- *Bacillus subtilis*		*B. subtilis*+	
		- *Pseudomonas aeruginosa*		*P. aeruginosa* +	
		- *Proteus mirabilis*		*P. mirabilis* +	
		- *Escherichia coli*		*E. coli* +	
Cassia alata fresh leave	60.0–80.0 nm	- *Escherichia coli*	-	*E. coli* ++	(Happy et al., 2019)
Cassia fistula	5.0–15.0 nm	- *Klebsiellaaerogenes*	-	*K. aerogenes* ++	(Suresh et al., 2015a)
		- *Escherichia coli*		*E. coli* +	
		- *Plasmodium desmolyticum*		*P. desmolyticum* +	
		- *Staphylococcus aureus*		*S. aureus* +	
Ceropegia candelabrum leaf extract	12–35 nm	- *Staphylococcus aureus*	-	*B. subtilis* ++	(Murali et al., 2017)
		- *Bacillus subtilis*		*S. aureus* +	
		- *Escherichia coli*		*E. coli*	
Cinnamomum Verum	45.0 nm	- *Staphylococcus aureus*	-	*S. aureus* ++	(Ansari et al., 2020)
		- *Escherichia coli*		*E. coli*+	
C. halicacabum leaf extract	65.0, 62.0, 55.0, and 48.0 nm	- *Staphylococcus saprophyticus*	-	*E. coli* ++	(Nithya and Kalyanasundharam, 2019)
		- *Bacillus subtilis*		*B. subtilis*++	
		- *Escherichia coli*		*S. saprophyticus* +	
		- *Pseudomonas aeruginosa*		*P. aeruginosa*	
Euphorbia hirta leaves extract	-	- *Streptococcus mutans*	-	*S. aureus* ++	(Ahmad and Kalra, 2020)
		- *Streptococcus aureus*		*S. mutans* +	
		- *Clostridium absonum*		*C. absonum* +	
		- *Escherichia coli*		*E. coli* +	
Ginger rhizome (*Zingiber officinale*)	23.0–26.0 nm	- *Klebsiella pneumonia*	-	*K. pneumonia* ++	(Janaki et al., 2015)
		- *Staphylococcus aureus*		*S. aureus*+	
Melia azedarach leaf extract	33–96 nm	- *Escherichia coli*	-	*P. aeruginosa*++	(Dhandapani et al., 2020)
		- *Staphylococcus aureus*		*S. thalpophilum*++	
		- *Pseudomonas aeruginosa*		*E. coli* +	
		- *Sphingobacterium. thalpophilum*		*S. aureus* +	
		- *Bacillus subtilis*		*K. pneumoniae*+	
		- *Klebsiella Pneumoniae*			
Pandanus odorifer leaf extract	90.0 nm	- *Bacillus subtilis*	-	*B. subtilis*++	(Hussain et al., 2019)
		- *Escherichia coli*		*E. coli* +	
Pomegranate (Punica granatum) leaves and flowers	57.75 and 52.50 nm	- *Bacillus cereus*	-	*E. faecalis* ++	(Ifeanyichukwu et al., 2020)
		- *Aeromonas hydrophila*		*S. diarizonae*++	
		- *Salmonella diarizonae*		*B. cereus* +	
		- *Enterococcus faecalis*		*A. hydrophila* +	
Ruta graveolens	28.0 nm	- *Pseudomonas desmolyticum*	-	*P. desmolyticum* ++	(Lingaraju et al., 2016)
		- *Klebsiella aerogenes*		*E. coli* +	
		- *Staphylococcus aureus*		*K. aerogenes* +	
		- *Escherichia coli*		*S. aureus* +	
Solanum nigrum leaf extract	20–30.0 nm	- *Staphylococcus aureus*	-	*S. aureus* ++	(Ramesh et al., 2015)
		- *Salmonella paratyphi*		*S. paratyphi* ++	
		- *Vibrio cholerae*		*V. cholerae* +	
		- *Escherichia coli*		*E. coli* +	

(*continued on next page*)

Table 2 (*continued*)

Type of plants extract	Size of nanoparticles	Type of bacteria	Antioxidant assay	Efficiency	References
Trifolium pratense flower extract	60.0–70.0 nm	- *Staphylococcus aureus*	-	*P. aeruginosa* ++	(Dobrucka and Dlugaszewska, 2016)
		- *Pseudomonas aeruginosa*		*S. aureus* +	
		- *Escherichia coli*		*E. coli* +	

++ more efficient, + efficient.

Table 3. Comparison of the antibacterial and antioxidant activities of Ag/ZnO from different plant extracts with other reported studies.

Type of plants extract	Size of nanoparticles	Type of bacteria	Antioxidant assay	Efficiency	References
Trigonella foenum-graecum leaf	75.0 nm	-*Staphylococcus aureus* -*Escherichia coli*	-	*S. aureus* ++ *E. coli* +	(Noohpisheh et al., 2020)
Bidens pilosa extract	2.20 nm	-*Escherichia coli* -*Staphylococcus aureus*	-	*E. coli* ++ *S. aureus* +	(Kyomuhimbo et al., 2019)
Macrotyloma Uniflorum	91.17 nm	-*Bacillus subtilis* -*Escherichia coli*	-	*B. subtilis* ++ *E. coli*+	(Sali et al., 2021)
Neem leaf Extract	35.0 nm	-*Pseudomonas aeruginosa* -*Staphylococcus aureus*	-	*P. aeruginosa* ++ *S. aureus* +	(Taha et al., 2020)
Verbascum speciosum	45.58 nm	-*Staphylococcus aureus* -*Escherichia coli*	-	*E. coli* ++ *S. aureus* +	(Mousavi-Kouhi et al., 2021)

++more efficient, +efficient.

including superoxide and hydroxyl radicals. This is due to the electrostatic attraction as well as their affinity to sulphur containing proteins within the bacteria. Thus, the nanoparticles ions are capable of adhering to the cell wall and cytoplasmic membrane of the bacteria. Within the bacteria, they modulate the microbial signal transduction pathways. In the current report, the growth inhibition by ZnO and Ag/ZnO may be ascribed to the cell membrane disruption and the expulsion of cytoplasmic contents from the bacteria, culminating to its death (Divyapriya et al., 2014).

3.5.2. Antioxidant activity

The antioxidant activity of the ZnO and Ag/ZnO was assessed using the DPPH method as a free radical, which is dominantly used due to its abundant free radicals. The DPPH assay is simple and a high potential method for scavenging free radicals during the examination of antioxidant activity of various nanoparticles (Zare et al., 2019). Figure 9 is a result of a radical scavenging activity of the test nanoparticles in comparison with the standard (ascorbic acid) against DPPH free radicals. As expected, the highest radical scavenging activity was observed at the highest concentration of all test samples including the standard. The ZnO, in contrast to the Ag/ZnO-NPs, was found to have a strong scavenging activity. This might be because ZnO crystallinity enhanced the amorphous nature of Ag/ZnO, which decreased Ag/ZnO antioxidant's capacity relative to ZnO while increasing the surface area to volume ratio. A large surface area to volume ratio of NPs typically results in high material performance (Srijampa, 2020) due to the high reactivity of the material's surface atoms. Usually, Ag and ZnO NPs are better able to donate hydrogen ions' electrons to DPPH free radicals, which subsequently results in higher radical scavenging activity (Suresh et al., 2015b). However, the opposite was observed in the current study. Consequently, the findings of the current study contradict those reported in (Khan et al., 2022; Noohpisheh et al., 2020) whereby Ag/ZnO exhibited higher antioxidant activity than ZnO nanoparticles.

4. Conclusions

ZnO nanoparticles and Ag/ZnO nanocomposite have been successfully prepared using a cost-effective, non-toxic, easy-to-handle, facile green approach using bulb extract of *U. epigea*. No external reagents or

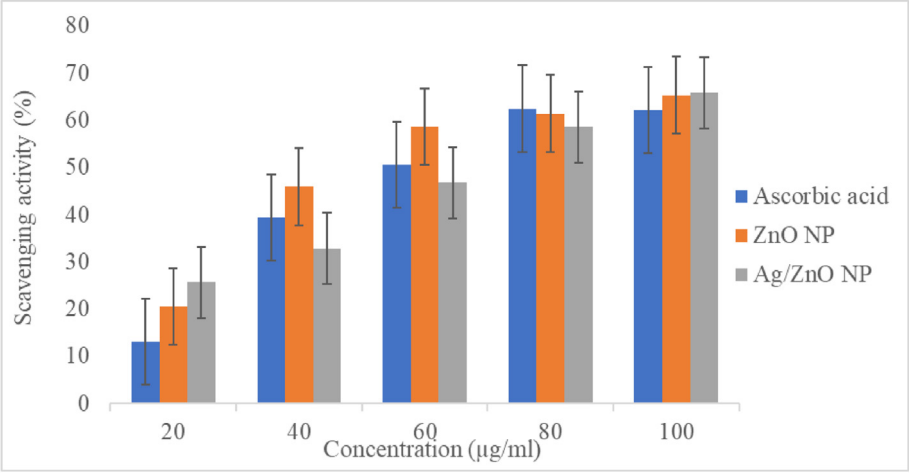

Figure 9. Scavenging activity of ZnO and Ag/ZnO nanoparticles against DPPH.

additives were added, and it only required temperature and pH control. The crystalline phases of the produced nanoparticles were confirmed by XRD, while FTIR analysis identified the functional groups present in the biomolecules of the *U. epigea* bulb. The elemental composition of ZnO and Ag/ZnO NPs was confirmed by EDX. The plant extract functions as a reducing agent for the Ag nanoparticles and mediator for the formation of the ZnO and its composite with Ag. The size of the synthesized nanoparticles contributed to their antibacterial activity and adding silver to ZnO nanoparticles enhanced its antibacterial activity. The antioxidant capacity of ZnO and Ag/ZnO might have been improved by the phenolic compounds found in *U. epigea*. The biogenic method enables the preparation of nanoparticles for biological purposes. The synthesis strategy may be extended to other metal oxide nanoparticles as a more effective approach compared to the physical and chemical routes.

Declarations

Author contribution statement

Martha Cebile Jobe: Performed the experiments; Analyzed and interpreted the data; Wrote the paper.

Doctor M.N. Mthiyane: Conceived and designed the experiments; Wrote the paper.

Mulunda Mwanza: Contributed reagents, materials, analysis tools or data.

Damian C. Onwudiwe: Conceived and designed the experiments; Analyzed and interpreted the data; Contributed reagents, materials, analysis tools or data; Wrote the paper.

Funding statement

Martha Cebile Jobe was supported by NWU through the award of a PhD bursary.

Data availability statement

Data will be made available on request.

Declaration of interest's statement

The authors declare no conflict of interest.

Additional information

No additional information is available for this paper.

References

Agarwal, H., Kumar, S.V., Rajeshkumar, S., 2017. A review on green synthesis of zinc oxide nanoparticles–An eco-friendly approach. Res.-Effic. Technol. 3, 406–413.

Agnihotri, S., Bajaj, G., Mukherji, S., Mukherji, S., 2015. Arginine-assisted immobilization of silver nanoparticles on ZnO nanorods: an enhanced and reusable antibacterial substrate without human cell cytotoxicity. Nanoscale 7, 7415–7429.

Ajitha, B., Reddy, Y.A.K., Reddy, P.S., 2015. Green synthesis and characterization of silver nanoparticles using Lantana camara leaf extract. Mater. Sci. Eng. C 49, 373–381.

Álvarez-Chimal, R., García-Pérez, V.I., Álvarez-Pérez, M.A., Tavera-Hernández, R., Reyes-Carmona, L., Martínez-Hernández, M., Arenas-Alatorre, J.A., 2022. Influence of the particle size on the antibacterial activity of green synthesized zinc oxide nanoparticles using Dysphania ambrosioides extract, supported by molecular docking analysis. Arab. J. Chem. 15, 103804.

Ansari, M.A., Murali, M., Prasad, D., Alzohairy, M.A., Almatroudi, A., Alomary, M.N., Udayashankar, A.C., Singh, S.B., Asiri, S.M.M., Ashwini, B.S., Gowtham, H.G., Kalegowda, N., Amruthesh, K.N., Lakshmeesha, T.R., Niranjana, S.R., 2020. Cinnamomum verum bark extract mediated green synthesis of ZnO nanoparticles and their antibacterial potentiality. Biomolecules 10, 336.

Assadpour, E., Mahdi Jafari, S., 2019. A systematic review on nanoencapsulation of food bioactive ingredients and nutraceuticals by various nanocarriers. Crit. Rev. Food Sci. Nutr. 59, 3129–3151.

Awwad, A.M., Amer, M.W., Salem, N.M., Abdeen, A.O., 2020. Green synthesis of zinc oxide nanoparticles (ZnO-NPs) using Ailanthus altissima fruit extracts and antibacterial activity. Chem. Int. 6, 151–159.

Barrientos-Velázquez, A.L., Arteaga, S., Dixon, J.B., Deng, Y., 2016. The effects of pH, pepsin, exchange cation, and vitamins on aflatoxin adsorption on smectite in simulated gastric fluids. Appl. Clay Sci. 120, 17–23.

Buetler, T.M., Gallagher, E.P., Wang, C., Stahl, D.L., Hayes, J.D., Eaton, D.L., 1995. Induction of phase I and phase II drug-metabolizing enzyme mRNA, protein, and activity by BHA, ethoxyquin, and oltipraz. Toxicol. Appl. Pharmacol. 135, 45–57.

Chaudhary, A., Kumar, N., Kumar, R., Salar, R.K., 2018. Antimicrobial activity of zinc oxide nanoparticles synthesized from Aloe vera peel extract. SN Appl. Sci. 1, 136.

Das, B., Khan, M., Jayabalan, R., Behera, S.K., Yun, S.-I., Tripathy, S.K., Mishra, A., 2016. Understanding the antifungal mechanism of Ag@ ZnO core-shell nanocomposites against Candida krusei. Sci. Rep. 6, 1–12.

De Sousa, L.Q., Da Conceição Machado, K., De Carvalho Oliveira, S.F., Da Silva Araújo, L., Dos Santos Monção-Filho, E., De Carvalho Melo-Cavalcante, A.A., Vieira-Júnior, G.M., Ferreira, P.M.P., 2017. Bufadienolides from amphibians: a promising source of anticancer prototypes for radical innovation, apoptosis triggering and Na+/K+-ATPase inhibition. Toxicon 127, 63–76.

Dima, C., Assadpour, E., Dima, S., Jafari, S.M., 2020. Bioactive-loaded nanocarriers for functional foods: from designing to bioavailability. Curr. Opin. Food Sci. 33, 21–29.

Divya, M., Sowmia, C., Joona, K., Dhanya, K., 2013. Synthesis of zinc oxide nanoparticle from Hibiscus rosa-sinensis leaf extract and investigation of its antimicrobial activity. Res. J. Pharm. Biol. Chem 4, 1137–1142.

Divyapriya, S., Sowmia, C., Sasikala, S., 2014. Synthesis of zinc oxide nanoparticles and antimicrobial activity of Murraya Koenigii. World J. Pharm. Pharmaceut. Sci. 3, 1635–1645.

Dobrucka, R., Długaszewska, J., 2016. Biosynthesis and antibacterial activity of ZnO nanoparticles using Trifolium pratense flower extract. Saudi J. Biol. Sci. 23, 517–523.

Elemike, E.E., Onwudiwe, D.C., Ekennia, A.C., Ehiri, R.C., Nnaji, N.J., 2017. Phytosynthesis of silver nanoparticles using aqueous leaf extracts of Lippia citriodora: antimicrobial, larvicidal and photocatalytic evaluations. Mater. Sci. Eng. C 75, 980–989.

El-Bahr, S., 2015. Effect of curcumin on hepatic antioxidant enzymes activities and gene expressions in rats intoxicated with aflatoxin B1. Phytother Res. 29, 134–140.

Fahimmunisha, B.A., Ishwarya, R., Alsalhi, M.S., Devanesan, S., Govindarajan, M., Vaseeharan, B., 2020. Green fabrication, characterization and antibacterial potential of zinc oxide nanoparticles using Aloe socotrina leaf extract: a novel drug delivery approach. J. Drug Deliv. Sci. Technol. 55, 101465.

Feris, K., Otto, C., Tinker, J., Wingett, D., Punnoose, A., Thurber, A., Kongara, M., Sabetian, M., Quinn, B., Hanna, C., 2010. Electrostatic interactions affect nanoparticle-mediated toxicity to gram-negative bacterium Pseudomonas aeruginosa PAO1. Langmuir 26, 4429–4436.

Fouladi-Fard, R., Aali, R., Mohammadi-Aghdam, S., Mortazavi-Derazkola, S., 2022. The surface modification of spherical ZnO with Ag nanoparticles: a novel agent, biogenic synthesis, catalytic and antibacterial activities. Arab. J. Chem. 15, 103658.

Gao, H., Popescu, R., Kopp, B., Wang, Z., 2011. Bufadienolides and their antitumor activity. Nat. Prod. Rep. 28, 953–969.

Goossens, J., Vandenbroucke, V., Pasmans, F., DE Baere, S., Devreese, M., Osselaere, A., Verbrugghe, E., Haesebrouck, F., DE Saeger, S., Eeckhout, M., 2012. Influence of mycotoxins and a mycotoxin adsorbing agent on the oral bioavailability of commonly used antibiotics in pigs. Toxins 4, 281–295.

Guengerich, F.P., Johnson, W.W., Shimada, T., Ueng, Y.-F., Yamazaki, H., Langouët, S., 1998. Activation and detoxication of aflatoxin B1. Mutat. Res. Fund Mol. Mech. Mutagen 402, 121–128.

Gunalan, S., Sivaraj, R., Rajendran, V., 2012. Green synthesized ZnO nanoparticles against bacterial and fungal pathogens. Prog. Nat. Sci.: Mater. Int. 22, 693–700.

Gupta, J., Mohapatra, J., Bahadur, D., 2017. Visible light driven mesoporous Ag-embedded ZnO nanocomposites: reactive oxygen species enhanced photocatalysis, bacterial inhibition and photodynamic therapy. Dalton Trans. 46, 685–696.

Happy, A., Soumya, M., Venkat Kumar, S., Rajeshkumar, S., Sheba, R.D., Lakshmi, T., Deepak Nallaswamy, V., 2019. Phyto-assisted synthesis of zinc oxide nanoparticles using Cassia alata and its antibacterial activity against Escherichia coli. Biochemistry and Biophysics Reports 17, 208–211.

Haque, M.A., Wang, Y., Shen, Z., Li, X., Saleemi, M.K., He, C., 2020. Mycotoxin contamination and control strategy in human, domestic animal and poultry: a review. Microb. Pathog. 142, 104095.

Hayes, J., Judah, D., Mclellan, L., Kerr, L., Peacock, S., Neal, G., 1991a. Ethoxyquin-induced resistance to aflatoxin B1 in the rat is associated with the expression of a novel alpha-class glutathione S-transferase subunit, Yc2, which possesses high catalytic activity for aflatoxin B1-8, 9-epoxide. Biochem. J. 279, 385–398.

Hayes, J.D., Judah, D.J., Mclellan, L.I., Neal, G.E., 1991b. Contribution of the glutathione S-transferases to the mechanisms of resistance to aflatoxin B1. Pharmacol. Ther. 50, 443–472.

Huh, A.J., Kwon, Y.J., 2011. Nanoantibiotics": a new paradigm for treating infectious diseases using nanomaterials in the antibiotics resistant era. J. Contr. Release 156, 128–145.

Hussain, A., Oves, M., Alajmi, M.F., Hussain, I., Amir, S., Ahmed, J., Rehman, M.T., EL-Seedi, H.R., Ali, I., 2019. Biogenesis of ZnO nanoparticles using Pandanus odorifer leaf extract: anticancer and antimicrobial activities. RSC Adv. 9, 15357–15369.

Ifeanyichukwu, U.L., Fayemi, O.E., Ateba, C.N., 2020. Green synthesis of zinc oxide nanoparticles from pomegranate (punica granatum) extracts and characterization of their antibacterial activity. Molecules 25, 4521.

Jain, D., Bhojiya, A.A., Singh, H., Daima, H.K., Singh, M., Mohanty, S.R., Stephen, B.J., Singh, A., 2020. Microbial fabrication of zinc oxide nanoparticles and evaluation of their antimicrobial and photocatalytic properties. Front. Chem. 8, 778.

Janaki, A.C., Sailatha, E., Gunasekaran, S., 2015. Synthesis, characteristics and antimicrobial activity of ZnO nanoparticles. Spectrochim. Acta Mol. Biomol. Spectrosc. 144, 17–22.

Jayachandran, A., Aswathy, T., Nair, A.S., 2021. Green synthesis and characterization of zinc oxide nanoparticles using Cayratia pedata leaf extract. Biochemistry and Biophysics Reports 26, 100995.
Kamboj, A., Rathour, A., Kaur, M., 2013. Bufadienolides and their medicinal utility: a review. Int. J. Pharm. Pharmaceut. Sci. 5, 20–27.
Khan, M.S., Dhavan, P.P., Ratna, D., Shimpi, N.G., 2022. Ultrasonic-assisted biosynthesis of ZnO nanoparticles using Sonneratia alba leaf extract and investigation of its photocatalytic and biological activities. J. Cluster Sci. 33, 1007–1023.
Kihal, A., Rodríguez-Prado, M.E., Cristofol, C., Calsamiglia, S., 2021. Quantification of the effect of mycotoxin binders on the bioavailability of fat-soluble vitamins in vitro. Animals 11, 2251.
Kim, J.S., Kuk, E., Yu, K.N., Kim, J.-H., Park, S.J., Lee, H.J., Kim, S.H., Park, Y.K., Park, Y.H., Hwang, C.-Y., 2007. Antimicrobial effects of silver nanoparticles. Nanomed. Nanotechnol. Biol. Med. 3, 95–101.
Kolodziejczyk-Czepas, J., Stochmal, A., 2017. Bufadienolides of Kalanchoe species: an overview of chemical structure, biological activity and prospects for pharmacological use. Phytochemistry Rev. 16, 1155–1171.
Koorbanally, N.A., Koorbanally, C., Harilal, A., Mulholland, D.A., Crouch, N.R., 2004. Bufadienolides from drimia robusta and Urginea epigea (hyacinthaceae). Phytochemistry 65, 3069–3073.
Koshani, R., Jafari, S.M., 2019. Ultrasound-assisted preparation of different nanocarriers loaded with food bioactive ingredients. Adv. Colloid Interface Sci. 270, 123–146.
Kyomuhimbo, H.D., Michira, I.N., Mwaura, F.B., Derese, S., Feleni, U., Iwuoha, E.I., 2019. Silver–zinc oxide nanocomposite antiseptic from the extract of bidens pilosa. SN Appl. Sci. 1, 1–17.
Lauridsen, C., 2019. From oxidative stress to inflammation: redox balance and immune system. Poultry Sci. 98, 4240–4246.
Lee, M., Lin, W., Lee, T., 2019. Potential crosstalk of oxidative stress and immune response in poultry through phytochemicals—a review. Asian-Australas. J. Anim. Sci. 32, 309.
Limaye, A., Yu, R.-C., Chou, C.-C., Liu, J.-R., Cheng, K.-C., 2018. Protective and detoxifying effects conferred by dietary selenium and curcumin against AFB1-mediated toxicity in livestock: a review. Toxins 10, 25.
Liu, Q., Li, J., Zhong, X., Dai, Z., Lu, Z., Yang, H., Chen, R., 2018. Enhanced antibacterial activity and mechanism studies of Ag/Bi2O3 nanocomposites. Adv. Powder Technol. 29, 2082–2090.
Liu, Q., Liu, E., Li, J., Qiu, Y., Chen, R., 2020. Rapid ultrasonic-microwave assisted synthesis of spindle-like Ag/ZnO nanostructures and their enhanced visible-light photocatalytic and antibacterial activities. Catal. Today 339, 391–402.
Lu, Z., Gao, J., He, Q., Wu, J., Liang, D., Yang, H., Chen, R., 2017. Enhanced antibacterial and wound healing activities of microporous chitosan-Ag/ZnO composite dressing. Carbohydr. Polym. 156, 460–469.
Lukhoba, C.W., Simmonds, M.S., Paton, A.J., 2006. Plectranthus: a review of ethnobotanical uses. J. Ethnopharmacol. 103, 1–24.
Manson, M.M., Ball, H., Barrett, M.C., Clark, H.L., Judah, D.J., Williamson, G., Neal, G.E., 1997. Mechanism of action of dietary chemoprotective agents in rat liver: induction of phase I and II drug metabolizing enzymes and aflatoxin B1 metabolism. Carcinogenesis 18, 1729–1738.
Mavrommatis, A., Giamouri, E., Tavrizelou, S., Zacharioudaki, M., Danezis, G., Simitzis, P.E., Zoidis, E., Tsiplakou, E., Pappas, A.C., Georgiou, C.A., 2021. Impact of mycotoxins on animals' oxidative status. Antioxidants 10, 214.
Milbury, P.E., Graf, B., Curran-Celentano, J.M., Blumberg, J.B., 2007. Bilberry (Vaccinium myrtillus) anthocyanins modulate heme oxygenase-1 and glutathione S-transferase-pi expression in ARPE-19 cells. Investig. Ophthalmol. Vis. Sci. 48, 2343–2349.
Milićević, D.R., Škrinjar, M., Baltić, T., 2010. Real and perceived risks for mycotoxin contamination in foods and feeds: challenges for food safety control. Toxins 2, 572–592.
Morones, J.R., Elechiguerra, J.L., Camacho, A., Holt, K., Kouri, J.B., Ramírez, J.T., Yacaman, M.J., 2005. The bactericidal effect of silver nanoparticles. Nanotechnology 16, 2346.
Mousavi-Kouhi, S.M., Beyk-Khormizi, A., Amiri, M.S., Mashreghi, M., Taghavizadeh Yazdi, M.E., 2021. Silver-zinc oxide nanocomposite: from synthesis to antimicrobial and anticancer properties. Ceram. Int. 47, 21490–21497.
Murali, M., Mahendra, C., Nagabhushan Rajashekar, N., Sudarshana, M.S., Raveesha, K.A., Amruthesh, K.N., 2017. Antibacterial and antioxidant properties of biosynthesized zinc oxide nanoparticles from Ceropegia candelabrum L. – an endemic species. Spectrochim. Acta Mol. Biomol. Spectrosc. 179, 104–109.
Noohpisheh, Z., Amiri, H., Farhadi, S., Mohammadi-Gholami, A., 2020. Green synthesis of Ag-ZnO nanocomposites using Trigonella foenum-graecum leaf extract and their antibacterial, antifungal, antioxidant and photocatalytic properties. Spectrochim. Acta, Part A 240, 118595.
Ocsoy, I., Paret, M.L., Ocsoy, M.A., Kunwar, S., Chen, T., You, M., Tan, W., 2013. Nanotechnology in plant disease management: DNA-directed silver nanoparticles on graphene oxide as an antibacterial against Xanthomonas perforans. ACS Nano 7, 8972–8980.
Paul, K.K., 2017. Role of surface plasmons and hot electrons on the multi-step photocatalytic decay by defect enriched Ag@TiO2 nanorods under visible light. J. Phys. Chem. C 121, 20016–20030.
Pierron, A., Alassane-Kpembi, I., Oswald, I.P., 2016. Impact of mycotoxin on immune response and consequences for pig health. Animal Nutrition 2, 63–68.
Rajaboopathi, S., Thambidurai, S., 2019. Synthesis of bio-surfactant based Ag/ZnO nanoparticles for better thermal, photocatalytic and antibacterial activity. Mater. Chem. Phys. 223, 512–522.
Rezaei, A., Fathi, M., Jafari, S.M., 2019. Nanoencapsulation of hydrophobic and low-soluble food bioactive compounds within different nanocarriers. Food Hydrocolloids 88, 146–162.
Sali, R.K., Pujar, M.S., Patil, S., Sidarai, A.H., 2021. Green synthesis of ZnO and Ag-ZnO nanoparticles using macrotyloma uniflorum: evaluation of antibacterial activity. Adv. Mater. Lett. 12, 1–7.
Samberg, M.E., Orndorff, P.E., Monteiro-Riviere, N.A., 2011. Antibacterial efficacy of silver nanoparticles of different sizes, surface conditions and synthesis methods. Nanotoxicology 5, 244–253.
Saramas, D., Ekgasit, S., 2021. Nano-zinc oxide-doped activated carbon from popped rice and its application for feed additive. Eng. J. 25, 41–50.
Satyavani, K., Gurudeeban, S., Ramanathan, T., Balasubramanian, T., 2011. Biomedical potential of silver nanoparticles synthesized from calli cells of Citrullus colocynthis (L.) Schrad. J. Nanobiotechnol. 9, 43.
Senthilraja, A., Krishnakumar, B., Hariharan, R., Sobral, A.J., Surya, C., John, N.A.A., Shanthi, M., 2018. Synthesis and characterization of bimetallic nanocomposite and its photocatalytic, antifungal and antibacterial activity. Separ. Purif. Technol. 202, 373–384.
Sharma, S., Kumar, K., Thakur, N., Chauhan, S., Chauhan, M.S., 2019. The effect of shape and size of ZnO nanoparticles on their antimicrobial and photocatalytic activities: a green approach. Bull. Mater. Sci. 43, 20.
Sondi, I., Salopek-Sondi, B., 2004. Silver nanoparticles as antimicrobial agent: a case study on E. coli as a model for Gram-negative bacteria. J. Colloid Interface Sci. 275, 177–182.
Suresh, D., Nethravathi, P., Rajanaika, H., Nagabhushana, H., Sharma, S., 2015a. Green synthesis of multifunctional zinc oxide (ZnO) nanoparticles using Cassia fistula plant extract and their photodegradative, antioxidant and antibacterial activities. Mater. Sci. Semicond. Process. 31, 446–454.
Suresh, D., Shobharani, R.M., Nethravathi, P.C., Pavan Kumar, M.A., Nagabhushana, H., Sharma, S.C., 2015b. Artocarpus gomezianus aided green synthesis of ZnO nanoparticles: luminescence, photocatalytic and antioxidant properties. Spectrochim. Acta Mol. Biomol. Spectrosc. 141, 128–134.
Taha, A., Ben Aissa, M., DaNa, E., 2020. Green synthesis of an activated carbon-supported Ag and ZnO nanocomposite for photocatalytic degradation and its antibacterial activities. Molecules 25, 1586.
Tao, G., Cai, R., Wang, Y., Liu, L., Zuo, H., Zhao, P., Umar, A., Mao, C., Xia, Q., He, H., 2019. Bioinspired design of AgNPs embedded silk sericin-based sponges for efficiently combating bacteria and promoting wound healing. Mater. Des. 180, 107940.
Thema, F., Manikandan, E., Dhlamini, M., Maaza, M., 2015. Green synthesis of ZnO nanoparticles via Agathosma betulina natural extract. Mater. Lett. 161, 124–127.
Wu, A.G., Lu, J.-J., 2022. Herbal Medicines In the Treatment of Liver Diseases-Efficacy. In: Action Mechanisms and Clinical Application.
Xiao, X., Wu, Z.-C., Chou, K.-C., 2011. A multi-label classifier for predicting the subcellular localization of gram-negative bacterial proteins with both single and multiple sites. PLoS One 6, e20592.
Youssef, A.M., EL-Nahrawy, A.M., Abou Hammad, A.B., 2017. Sol-gel synthesis and characterizations of hybrid chitosan-PEG/calcium silicate nanocomposite modified with ZnO-NPs and (E102) for optical and antibacterial applications. Int. J. Biol. Macromol. 97, 561–567.
Zak, A.K., Abrishami, M.E., Majid, W.A., Yousefi, R., Hosseini, S., 2011. Effects of annealing temperature on some structural and optical properties of ZnO nanoparticles prepared by a modified sol–gel combustion method. Ceram. Int. 37, 393–398.
Zare, M., Namratha, K., Alghamdi, S., Mohammad, Y.H.E., Hezam, A., Zare, M., Drmosh, Q.A., Byrappa, K., Chandrashekar, B.N., Ramakrishna, S., Zhang, X., 2019. Novel green biomimetic approach for synthesis of ZnO-Ag nanocomposite; antimicrobial activity against food-borne pathogen, biocompatibility and solar photocatalysis. Sci. Rep. 9, 8303.